ORIGINAL PAPER

Molecular dynamics simulation of static crystallization and tensile deformation of bimodal HDPE/UHMWPE: Influence of long chain content

Fan Zhang, Jieqi Wang, Yangyang Zhao, Xuelian He*

Shanghai Key Laboratory of Multiphase Material Chemical Engineering, East China University of Science and Technology, Shanghai 200237, China

Corresponding Author: Xuelian He (E-mail: hexl@ecust.edu.cn)

Received: 2 April 2024, Accepted: 29 June 2024

DOI: 10.22063/POJ.2024.3596.1301

ABSTRACT

The effect of long chain content (X_L) on the static crystallization and tensile deformation mechanisms of bimodal HDPE/UHMWPE was investigated by molecular dynamics simulations. The crystallization of HDPE/UHMWPE undergoes three stages: nucleation, rapid growth of lamellar crystals, and stabilization. The increase of X_L leads to the formation of more nucleation sites, which promotes nucleation, but at the same time leads to an increase of entanglement sites, which is not conducive to the movement of the long chains to the growth front to fold and form lamellar crystals. Tensile deformation is performed on the crystallized models and the systems exhibit three stages: elastic deformation, plastic deformation and stress hardening. During deformation, the increase of X_L improves the orientation nucleation and crystallinity (X_c), but when X_L exceeds 4 wt%, the entanglement effect becomes more pronounced, leading to a decrease in X_c. The effect of temperature is also taken into account: at low temperatures, a suitable range (2-4 wt%) exists to optimize the mechanical properties of the material. At high temperatures, there is almost no stress-hardening phenomenon, but the addition of long chains has an impeding effect on the melting of the lamellar crystals, and when X_L is greater than 8 wt%, stress-induced melting is more likely to occur, accelerating the melting of the crystals.

Keywords: Molecular dynamics simulation, static crystallization, long chain content, nucleation, tensile deformation.

INTRODUCTION

The high-density polyethylene/ultra-high molecular weight polyethylene (HDPE/UHMWPE) system is a bimodal polyethylene (BMPE) with a bimodal molar mass distribution, and its structure is approximately two interpenetrating layered network structures [1-4]. In the system, UHMWPE [5-8], as the long chain part (high molecular weight), can provide excellent mechanical properties, such as resistance to slow crack growth (SCG) and ultra-long service life. HDPE [9], as a short chain part (low molecular weight), can improve processing properties. Bimodal polyethylene combines processing and mechanical properties, which has shown significant advantages in many key fields [10-12], such as manufacturing high-grade pipes for transporting water, gas, and sewage, high-strength fibers for mooring pipelines in offshore oil fields, and bulletproof and stab proof products, thus receiving widespread attention.

It was initially noted that by modulating the high and low molecular weight distribution of HDPE/UHMWPE, the materials could be made to meet the application requirements in different scenarios. Xu [13] used oscillatory shear injection molding (OSIM) to prepare HDPE/UHMWPE composites, and found that with the increase of the UHMWPE content in the blended matrix up to 30 wt%, the tensile strength of plain HDPE increased from 26.4 MPa to 68.5 MPa, while the impact strength increased from 6.3 kJ/m^2 to 34.1 kJ/m^2. It was attributed to the shear orientation effect caused by UHMWPE, which made the molecular orientation of the system more obvious, thus forming a higher content of tandem-crystal microstructures within the molecules. Wang [14] et al. added UHMWPE of different molecular weights (1-3 million) to HDPE matrix at a ratio of 5-40 wt%, and found that the yield strength improved with increasing molecular weight of UHMWPE, but there was an optimal range of UHMWPE concentration (5-10 wt%). When the UHMWPE content is greater than 10 wt%, the yield strength of the system tends to level off or even decrease slightly as the content increases. The explanation for this phenomenon is that the system produces a bulky spherical crystal structure, with significant interfaces between the spherical crystals, where internal stresses caused by differences in chain arrangement are present.

With the development of high-performance polyethylene products, there has been a growing interest in the effect of chain structure on the crystallization and stretching processes within its molecules [15-17]. For the crystallization process, Chen et al. [18] found that in the BMPE system, the long and short chains tend to nucleate and crystallize separately, which leads to a decrease in the probability of

generation of tie molecules and the formation of a discrete laminar network. Hsiao et al. [19-20] investigated the effect of different UHMWPE contents (0-10 wt%) on the crystallization process: a high UHMWPE content causes excessive local stress in the UHMWPE, which makes it easier to stretch and form a shish structure. Zhao et al. [21] found that in the wide molecular weight distribution system under a strong flow field, the intermolecular interaction force is weaker, which leads to the preferential formation of a large number of *trans*-enrichment of the extended long chains, which can accelerate the transformation of precursors into shish nuclei and the formation of lamellar crystals, and lamellar crystal structure is thicker and more regular and compact. For the stretching process, Li et al. [22] used in-situ synchrotron radiation to study the stretching mechanism of UHMWPE fibers: at low temperatures, crystal fragmentation plays a leading role in stress hardening; while at high temperatures, the stress hardening phenomenon is caused by the formation of highly oriented microfiber structures and oriented lace structures induced by stretching.

In recent years, simulation methods have been widely emphasized in order to deeply investigate the molecular mechanisms of crystallization and stretching of high-performance polyethylene systems and the influence of chain structure on these processes [23-27]. For the crystallization process, Sanmartín et al. [28] designed three types of models for linear *n*-alkanes and branched *n*-alkanes with symmetric distributions of methyl and butyl groups. By analyzing the conformations as well as quantitatively analyzing the induction time of nucleation, it was finally found that with the increase of the length of short branched chains, the short branched structure slows down the nucleation process and intensifies the blocking effect. He et al. [26] used molecular dynamics methods to study the effects of methylene sequence length, branched chain concentration, branched chain distribution, and branched chain length on the crystallization process of the bimodal polyethylene system, especially the formation of the precursor and the evolution of the nucleation process. It is shown that the methylene sequence length (MSL) of the system determines the induction time of the precursor, and there exists a critical length (MSL) of the nucleation methylene sequence, which is about 60 CH_2 units.

For tensile simulations, Rutledge et al. [29-33] constructed a model of polyethylene with alternating crystalline and amorphous regions, which was deformed in tension with the transverse dimensions and volume of the entire system remaining constant. The method was then extended to simulate different forms of plastic deformation, including tension, compression, and shear. Rutledge constructed polyethylene models with different transverse dimensions and performed tensile simulations at two

different strain rates. The results showed that the transverse dimension had little relation to the deformation behavior. In addition, at the faster strain rate, cavity formation dominated the deformation. At the slower strain rate, the stress-strain curve oscillated, and strain hardening was observed due to repeated melting and recrystallization of polyethylene. Hossain et al. [34] used the *Dreiding* II force field to investigate the effects of chain length, chain number and temperature on the deformation behavior of polyethylene and found that longer chains have a higher entanglement density and thus higher yield stress and more pronounced softening, while a decrease in temperature favors an increase in the modulus of elasticity and yield stress.

In our previous work [35,36], we had revised the molecular mechanism of tie-molecules at the onset of the steric crystallization for the branched bimodal HDPE chains through MD simulations. Moreover, we compensated the molecular mechanism of MWD on shish-kebab formation in HDPE under flow-induced crystallization considering Grubbs, metallocene, Ziegler-Natta and chromium-based catalysts [37-40]. The effect of branching topology on flow-induced precursors, shish nuclei and strings, and the laminar morphology of model chains of HDPE using precise bimodal HDPE was also explored. However, molecular dynamics studies on the crystallization and tensile deformation mechanisms of HDPE/UHMWPE systems are still lacking. In this work, bimodal HDPE/UHMWPE models with different long chain (UHMWPE chain) concentration were designed to explore (1) the influence of chain structure on the static crystallization process, and (2) the influence of chain structure and temperature on the tensile deformation process, aiming to lay the foundation for the development of high-performance HDPE/UHMWPE.

MODELS AND METHODS

Models

In this work, united-atom models of HDPE/UHMWPE with different long chain contents (X_L) are established by using Materials Studio™ and PACKMOL, and the influence of X_L on the crystallization and tensile deformation is studied. The short chain is composed of 100 CH_2 units, the long chain is 3000 CH_2 units, and the X_L is 0, 2, 4, 6, 8 and 10wt%. Table 1 summarizes the nomenclature and parameters of the six models. Taking L/S-r30-2 as an example, the model is named as follows: L/S-r30 means that

the long chain (L) contains 3000 CH_2 units, the short chain (S) contains 100 CH_2 units, and the molecular weight ratio of the long chain to the short chain is 30; -2 means that X_L is 2 wt%.

Table 1. Characteristics of HDPE/UHMWPE models with different long chain concentration X_L.

Models	[a]Total carbon number of short chain (HDPE)	[a]Total carbon number of long chain (UHMWPE)	Long chain concentration X_L (wt%)
L/S-r30-0[b]	100C	3000C	/
L/S-r30-2			2
L/S-r30-4			4
L/S-r30-6			6
L/S-r30-8			8
L/S-r30-10			10

[a] United-atom model, treating each methylene (CH_2) or methyl (CH_3) unit as an atom to simplify calculation. The mass of each methylene and methyl unit is 14 and 15 g mol^{-1}.

[b] In the L/S-r30-0 system, the long chain content is 0. This system only contains short chains.

Simulation details

In this work, our molecular dynamics simulation is a combination of GROMACS and LAMMPS. The force field in the GROMACS package helps us construct united-atom models and perform dynamic simulations, while LAMMPS software helps us perform stretching simulations and obtain molecular motion orbitals for analyzing the conformational evolution of molecular chains.

GROMACS and *Dreiding* II force field are used to simulate the crystallization kinetic process. Choi [41] discussed the effect of *Dreiding* II force field on the folding process of polymer chains and confirmed that the force field was suitable for polymer models with high crystallinity. The total energy (E_{total}) consists of two parts: (1) kinetic energy ($E_{kinetic}$), which is related to the static crystallization temperature; (2) potential energy ($E_{potential}$), expressed as $E_{potential} = E_{bond} + E_{angle} + E_{dihedral} + E_{vdW}$, where E_{bond} is bond stretching energy, E_{angle} is bond angle bending energy, $E_{dihedral}$ is dihedral angle torsion energy and E_{vdW} is non-bond potential energy.

The Lennard-Jones potential function in the *Dreiding* II force field [41,42] is used to calculate the interatomic interactions: $V(r) = 4\varepsilon\left[\left(\frac{\sigma}{r}\right)^{12} - \left(\frac{\sigma}{r}\right)^{6}\right]$. In the formula, r is the distance between atom i and j (the cutoff radius is 10.5 Å), ε is the depth of the potential well, σ It is the distance at which the interatomic forces disappear exactly. The *LJ* potential parameters used to describe specific united-atoms in the *Dreiding* II force field are shown in Table 2.

Table 2. *LJ* potential parameters of united atoms in the *Dreiding* II force field.

United-atom	Mass (g/mol)	Lennard–Jones well depth ε (kcal/mol)	Lennard–Jones well size σ (Å)
CH_2	14	1.046	0.369
CH_3	15	0.830	0.362

The molecular dynamics simulation consists of five steps: (1) energy minimization, (2) temperature equilibrium, (3) pressure equilibrium, (4) crystallization, and (5) uniaxial stretching. Periodic boundary condition is used in the simulation process, and *Verlet* algorithm with a time step of 2 fs is used to integrate the atomic motion equations to achieve energy convergence. The *NVT* ensemble and the *Nosé-Hoover* method are used to perform temperature equilibrium (T = 800 K, and the relaxation time is 10 ns with a time step of 1 fs). The *NPT* ensemble and the *Parrinello-Rahman* method are used to perform pressure equilibrium. The pressure is set to P = 1 atm and the relaxation time is 10 ns with a time step of 1 fs. For HDPE/UHMWPE, a static crystallization simulation process is used to reduce the conformation from T = 800 K to T = 300 K, with a relaxation time of 50 ns and a timestep of 1 fs. Then, the ordered conformation obtained by static crystallization is used as the input conformation of LAMMPS, and the relevant parameters of the *Dreiding* II force field are used for tensile deformation simulation. In this process, the *NPT* ensemble is used to perform temperature and pressure equilibrium first (10 ns with a timestep of 1 fs). The temperature parameters are selected as T = 100 K, 150 K, 200 K, 300 K and 400 K, and the pressure is set to P = 1 atm. Then the models are stretched along the Z-axis at a fixed engineering stretching rate of 1×10^{10}/ s (and the total simulation time is 300 ps with a timestep of 1 fs). When selecting the stretching rate, we find that as the stretching rate increases, the yield stress and modulus also increase. At higher stretching rates (1×10^{10}/s or 1×10^{11}/s), the stress-strain curve of HDPE/UHMWPE appears a short-term plateau after passing through the strain softening stage. The

stress remains unchanged as the strain increases, and then enters the strain hardening stage. However, at lower strain rates (1×10^{9}/s), no plateau was observed after strain softening, strain hardening occurred directly, and both strain softening and strain hardening became insignificant. In the current manuscript, we chose to perform tensile simulation of the system at a stretching rate of 1×10^{11}/s so that obvious strain softening and strain hardening phenomena can be observed in the stress-strain curve.

Data analysis methods

Interchain contact fraction (ICF)

In this work, interchain contact fraction (*ICF*) is calculated to quantify the density of the inter-atoms within a certain radius of HDPE/UHMWPE chains. It is defined as:

$$ICF = \frac{\sum_{N_{inter}}(r_l)}{\sum_{N_{total}}(r_l)} \tag{1}$$

where $N_{inter}(r_l)$ is the number of interchain atoms around certain atom at distance r, $N_{total}(r_l)$ is the number of total atoms around the same atom. The distance r_l ranging from 0.48 to 0.52 nm was chosen.

Site order parameter (SOP) and crystallinity (X_c)

Here the site order parameter (*SOP*) is used to quantitatively characterize the degree of order in oriented crystals [43-48]. The average order parameter of any two pairs of unit bond vectors surrounding a certain atom k in a spherical space of radius *R* is defined as SOP_k, and the formula is as follows:

$$SOP_k = \frac{\left\langle 3\cos^2\varphi - 1\right\rangle}{2} = \frac{3}{2}\left\langle \left(\vec{e}_i \cdot \vec{e}_j\right)^2 \right\rangle_R - \frac{1}{2} \tag{2}$$

where *i* and *j* are any two orientation vectors in the crystallographic domains within the sphere around that site. As reported in reference 42, Yang found that increasing the radius *R* had no significant effect on the *SOP* value of the crystal region, but it significantly decreased the *SOP* value of the amorphous region. When *R* was greater than 1.0 nm, the *SOP* value of the amorphous region was more accurate. But as *R* increases, the computation time increases exponentially. On the contrary, if the radius *R* is

reduced, the *SOP* in the amorphous region will increase significantly. Yang determined the value of *R* by means of a radial distribution function (*RDF*) curve (the first peak on the curve decreases to a local minimum at a distance of 0.7 nm). We used the same method to calculate *R* = 0.55 nm.

For a system consisting of *N* sites, the overall order parameter was calculated using the average SOP_k of all sites in the system:

$$SOP = \frac{1}{N}\sum_{i=1}^{N} SOP_k \quad (3)$$

Subsequently, the crystallinity X_c of the *semi*-crystalline polymer can be obtained by calculating the number of units with SOP_k greater than the critical value. The calculation formula is as follows:

$$X_c = \frac{N_{cv}}{N} \quad (4)$$

Here, N_{cv} represents the number of atoms (or CH_2 units) in the system whose site order parameter is greater than the critical value, and *N* is the total number of atoms (or CH_2 units) in the system.

The statistical methods for nucleation precursors, nuclei and crystal regions

After defining the crystallinity X_c, the crystalline region is the region composed of atoms (or CH_2 units) whose *SOP* is greater than the critical value. In the crystallization region, when the cosine average of the angles between any two bond vectors within a certain range is greater than a specific value (0.82), these CH_2 are considered to belong to the same crystal nucleus or crystal region. In the initial stage of the crystallization process, nucleation precursors will appear in the system, and these precursors will disappear, grow or fuse before becoming stable nuclei. In the study of Hu [24,25] and Yamamoto [49] et al., a precursor is defined as an unstable zigzag chain segment composed of at least eight or more consecutive bond vectors, with the angle between adjacent chord vectors less than 35° (or 30°). Therefore, the size of the precursor is defined in this work to be no less than 8 CH_2 units.

Trans-state population

The *trans*-state population is calculated by calculating the *trans*-dihedral angle probability (P_i). When the dihedral angle φ_k is 180° ± 15°, the dihedral angle at this time is considered to be the *trans*-dihedral angle φ_i, and the formula is as follows:

$$P_i = \frac{N_i}{\sum N_k} \quad (5)$$

Where N_k is the number of dihedral angles, and N_i represents the number of *trans*-dihedral angles in the entire system.

Tie molecule parameters

Amorphous chain segments that pass through two or more crystalline regions are defined as tie molecular segments. Tie molecules are located in the amorphous region and their role is to connect different crystalline regions. The formula for calculating the concentration of tie molecules P_c is:

$$P_c = \frac{N_t}{N} \quad (6)$$

In the formula, N_t is the number of atoms in the chain segment of the tie molecule, and N represents the number of atoms in the entire system.

The density of tie molecules P_d is the ratio of the number of atoms in the tie molecule chain segments to the number of atoms in the amorphous region:

$$P_d = \frac{P_c}{1 - X_c} \quad (7)$$

RESULTS AND DISCUSSION

ICF of HDPE/UHMWPE models with different long chain contents

In this work, we calculate *ICF* to quantify the density of the inter-atoms within a certain radius of different models. Figure 1 indicates the variation of the *ICF* of HDPE/UHMWPE models with different X_L with collapse time (t) in the interpenetration process. As can be seen from curves, the trend of all curves is almost the same. At first, the *ICF* of all systems rises sharply to a high value. When the collapse time is about 40 ps, the *ICF* of L/S-r30-0 is the highest, which indicates that HDPE/UHMWPE chains with lower X_L can penetrate each other more easily at a short notice. With the increase of collapse time, the *ICF* of all systems decreases slightly and tends to stable eventually. The *ICF* of six systems is different in the end: as X_L increases from 0 wt% to 10wt%, the *ICF* decreases from 0.88 to 0.73.

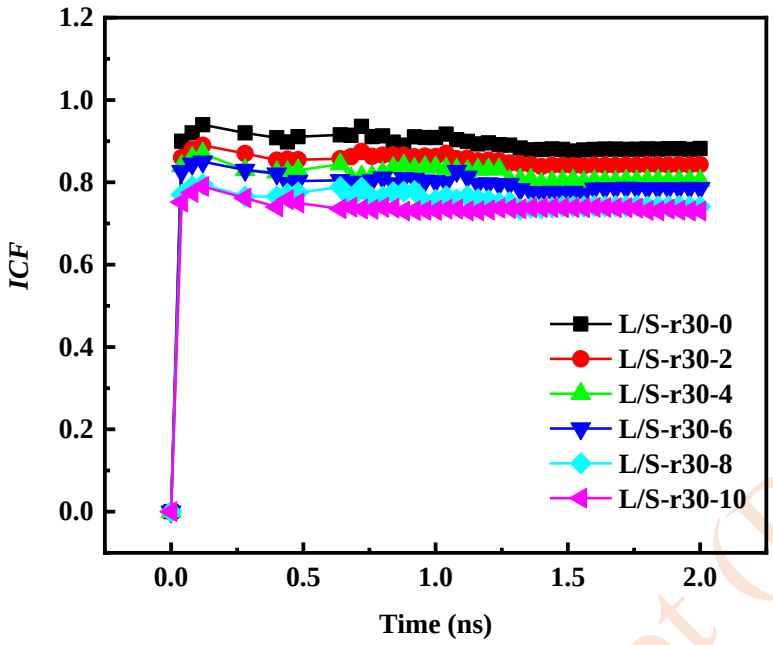

Figure 1. Interchain contact fraction (*ICF*) of HDPE/UHMWPE models with different long chain contents with collapsing time (t) at T = 800K.**3.2 Evolution of radius of gyration and density of HDPE/UHMWPE models**

We take the L/S-r30-10 system as an example to track the evolution of its radius of gyration (R_g) and density during MD simulation, as shown in Figure 2. R_g describes the degree of tightness of the molecular chains in the system. When the temperature drops from 800 K to 300 K, R_g decreases. At high temperatures, molecular chains have greater thermal mobility and R_g continues to change; At low temperatures, R_g is at a relatively stable value, indicating that the molecular chains are in a stable folded state. The density increases with the decrease of temperature. When the temperature drops from 800 K to 300 K, the system density increases from 0.88 g/cm^3 to 1.17 g/cm^3, which is close to the experimental data, indicating that the force field used is acceptable. There is a difference in the rate of the evolution of R_g and density with temperature, which reflects the transition in the system status.

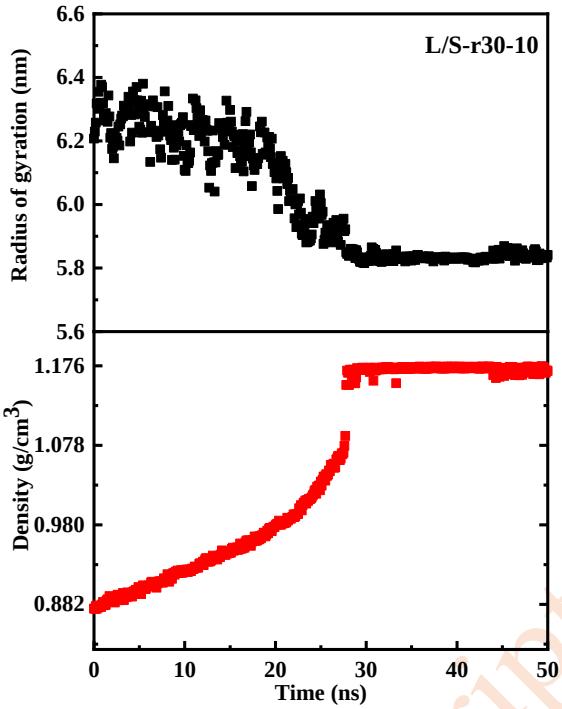

Figure 2. Evolution curves of radius of gyration and density for L/S-r30-10 model during MD simulation.

Crystallization process and mechanism of HDPE/UHMWPE models

Three-stage flow-induced crystallization of HDPE/UHMWPE

In our previous work [50], we proposed a three-step formation process of shish-kebab crystallites from linear polydisperse polyethylene systems under enhanced flow, including the emergence of precursors, the evolution from precursors to shish cores, and the formation of flake crystallites. Here, the three-step crystallization mode is also applicable to HDPE/UHMWPE. Figure 3 shows the *vdW* energy, crystallinity (X_c), site order parameter (*SOP*) and P_i as a function of time during the static crystallization process of HDPE/UHMWPE systems with different long chain contents. All models show the same trend, that is, as the crystallization process proceeds, the X_c, *SOP*, and P_i continue to increase to remain unchanged, and the *vdW* energy continues to decrease to a certain value.

Stage I (about 22 ns) is the *trans*-dihedral enrichment nucleation stage. The *vdW* energy decreases slowly and the P_i increases slightly, indicating that the dihedral angle of the polyethylene segment is continuously adjusted from random *trans*- and *gauche*- dihedral angles to *trans*-dihedral angles. *Trans*-dihedral enrichment and crystallization precursors (≥ 8C) are subsequently produced. In addition, compared with the P_i and *SOP*, X_c grows more slowly, indicating that after local *trans*-enrichment of the

chain segments, unstable small crystal region clusters in front of the crystal nucleus are formed. These clusters will undergo behaviors such as disintegration and merger, and gradually form a certain number of stable crystal nuclei.

Stages II and III (about 30 ns) are the rapid growth stages of lamellar crystals. Firstly, in stage II, small fragments of lamellar crystals grow gradually. With the increase of crystallization time, the P_i continues to grow, and its growth rate is significantly increased compared to stage I. This indicates that the *trans* enrichment phenomenon is intensified, and the *vdW* energy of the system continues to decrease, which results in the rapid formation of a large number of new small crystalline regions, and a significant increase in *SOP* and X_c. In stage III, the number of *trans*-dihedral angles increases dramatically and the *vdW* energy shows a large decrease, but the growth of S*OP* and X_c is not very obvious. This indicates that a large number of new crystalline regions are not formed rapidly, but due to the transformation of the bridging molecular chains at the interface of the small crystalline regions into *trans* dihedral angles and folding into the crystalline regions, resulting in the rapid fusion and merging of the small crystalline regions into a large crystalline region, which causes the system energy to decrease sharply. This evolution can be seen in the conformation of Figure 5, where slightly dispersed crystalline regions predominate at the end of stage II, whereas at the end of stage III the smaller crystalline regions merge into a continuous large crystalline region.

Stage IV is the stable stage after crystallization is completed. The P_i, X_c and *SOP* all tend to a certain stable value, which indicates that the crystal structure is basically complete. At this stage, the *vdW* energy remains basically unchanged, indicating that only subtle conformational adjustments occur between molecules, and the crystallization process basically reaches equilibrium.

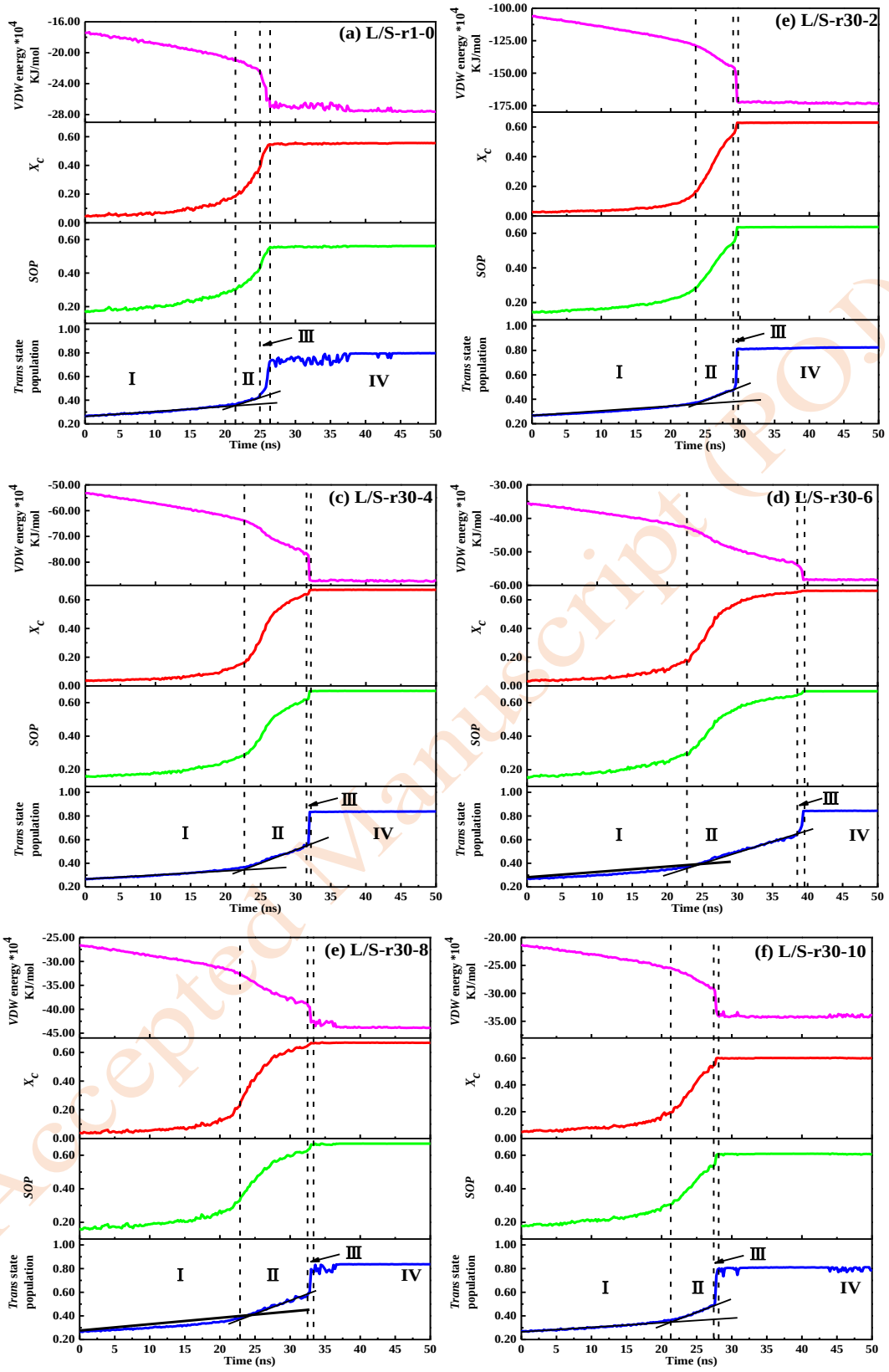

Figure 3. Evolution curves of *vdW* energy, X_c, *SOP* and *trans*-state population for HDPE/UHMPWE models with different long chain concentration: (a) 0, (b) 2, (c) 4, (d) 6, (e) 8 and (f) 10 wt%.

Figure 4 shows the curves of CH_2 units in the crystal region and P_i with time in HDPE/UHMWPE systems with different X_L. In the nucleation stage (I) there is no significant increase in the proportion of CH_2 units in the crystal region, and the slow increase of P_i indicates that there is almost no significant growth in the nucleus or in the crystal region, and most of them are small clusters of precursors aggregated by *trans*-enriched fragments. In the stage II of rapid crystal growth stage, the CH_2 units and P_i within the crystal region also increase rapidly, the molecular chains are folded and deposited at the growth front, and the small crystal region grows rapidly; in the stage III, the P_i increases sharply, and the CH_2 units still grow steadily, and in combination with the conformation in Figure 5, in this stage, the small crystal regions merge and merge rapidly into the large crystal region, and the *vdW* energy of the system decreases sharply. In the stabilization stage (IV), the basic parameters remain unchanged. It can be seen that for all systems, the rate of evolution of the P_i increases sharply from stage II to stage III, which is first observed in system with a long chain content of 0 wt%. At the same time, it can be seen that as X_L increases from 0 wt% to 6 wt%, the time for the growth of small crystal fragments to reach saturation gradually increases. While as X_L increases from 6 wt% to 10 wt%, the growth of small crystal fragments reaches saturation faster.

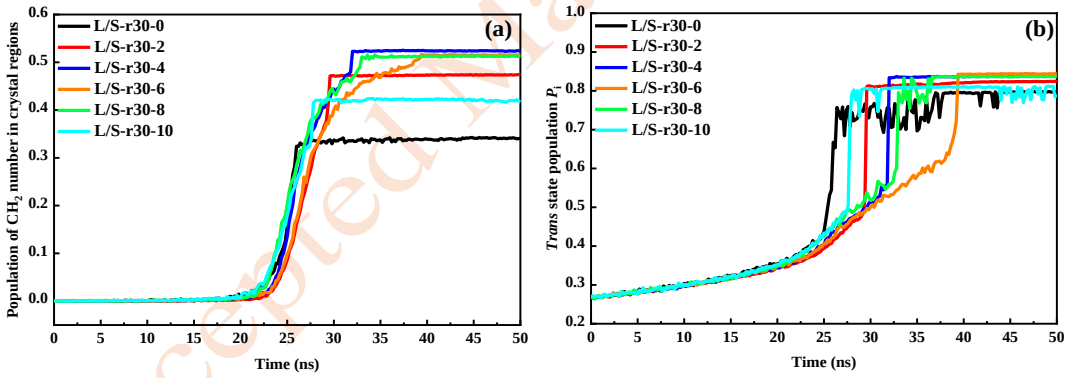

Figure 4. The curves of population of (a) CH_2 units involved in crystal regions and (b) *trans*-state population P_i with time for HDPE/UHMWPE with different long chain concentration X_L.

Taking the L/S-r30-2 chain model as an example, Figure 5 shows the conformational evolution of the condensed state of the molecular chain of bimodal HDPE/UHMWPE during the static crystallization process (red represents the crystalline region and blue represents the amorphous region). It can be clearly seen that in the nucleation stage I the crystal regions are smaller and dispersed, and the molecular chain segments in the crystal regions are shorter. From stage I to stage II, the molecular chain segments

gradually transform into the trans conformation, and the crystal regions gradually grow, forming a large number of small crystal region fragments. In stage III, the molecular chains between the interfaces quickly transform into regular fragments of *trans*-dihedral angles, and small crystalline fragments quickly integrate and merge to form large crystalline areas. In stage IV, crystallization is completed, the molecular chains in the crystal area are fine-tuned, and the structure of the crystal area is basically unchanged.

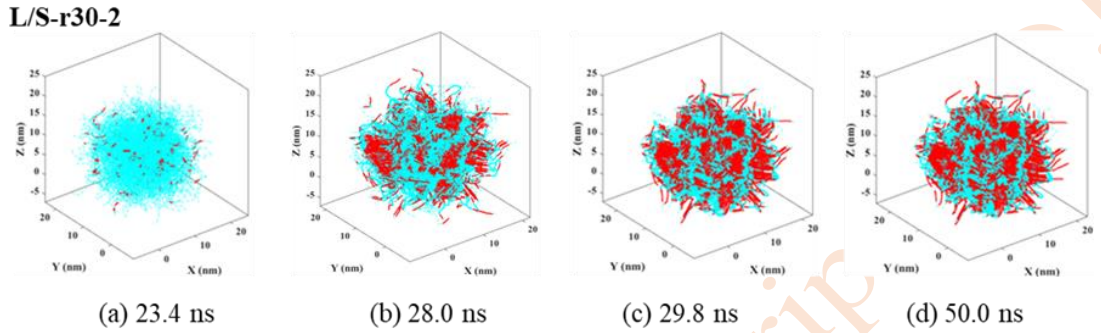

Figure 5. Evolution snapshots of the microstructure of L/S-r30-2 at (a) stage I (nucleus formation), (b) stage II (growth of small crystal fragments) and stage III (crystal regions mergence), and stage IV (stable stage).

Effect of long chain content on nucleation process and crystal growth stage

Figure 6 shows the time used for each stage and the variation of P_i with long chain content at the end of each stage. In the nucleation stage (I), the transition time and P_i were basically kept at 23 ns and 0.38. Compared with the pure HDPE system, the addition of long chains leads to a slight increase in the nucleation time. In the crystal growth stage (II & III), P_i increases and then decreases with the increase of long chain content, and the crystal growth time shows the same trend. This shows that as the X_L increases, more long chain segments fold into the crystal region and promote the growth of the crystal region. However, the long chains themselves move slowly, and the crystal growth takes a longer time. Therefore, as the content continues to increase ($\geq$ 6 wt%), the degree of chain entanglement increases, and many of the long chains instead fail to enter the folding into the crystal region, so that the P_i and the X_c both decrease. In addition, Figure 6 (b) shows the proportion of long chains involved in nucleation, and it is also found that with the increase of X_L, the proportion of long chain contribution in the CH_2 unit of the nucleus increases dramatically, especially when the content reaches and exceeds 8 wt%, which suggests that the long chains are able to contribute to the formation of stable nuclei, and provide a good environment for the rapid growth of lamellar crystals afterward.

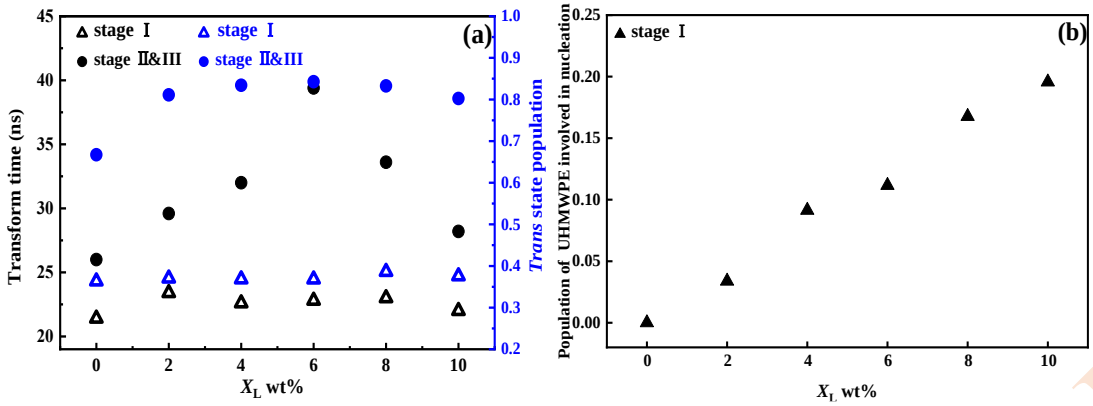

Figure 6. The variation of (a) nucleation time (I) and crystal growth time (II & III) (black) and *trans* state population (blue) at stage I (nucleus formation) and stage II & III (crystal growth) and (b) population of UHMWPE involved in nucleation with long chain concentration.

Effect of long chain content on platelet growth kinetics

Figure 7 exhibits the crystallization kinetic curves of HDPE/UHMWPE, while the curves of semi-crystallization time $t_{1/2}$ and crystallization rate G with X_L are obtained by using graphical method [51]. When crystallinity X_c = 50% (on the crystallization kinetics curve), the corresponding time is $t_{1/2}$. G = 1/ $t_{1/2}$ is defined which can more directly reflect the size of crystallization rate. We perform three repeated simulation calculations on $t_{1/2}$ and G for each system to obtain the average value. As shown in Figure 7(b), the lamellar crystal formation rate decreases and then raises with the increase of X_L. It reaches the minimun value when the X_L is 2 wt%. When the content is less than 6 wt%, the degree of entanglement increases due to the increase in the X_L, and the movement as well as folding of the long chains are restricted to a certain extent, resulting in a slowdown in the growth of lamellar crystals. And when the X_L is more than 6 wt%, the crystallization rate begins to increase, which is closely related to the evolution of the entangled structure of the polymer.

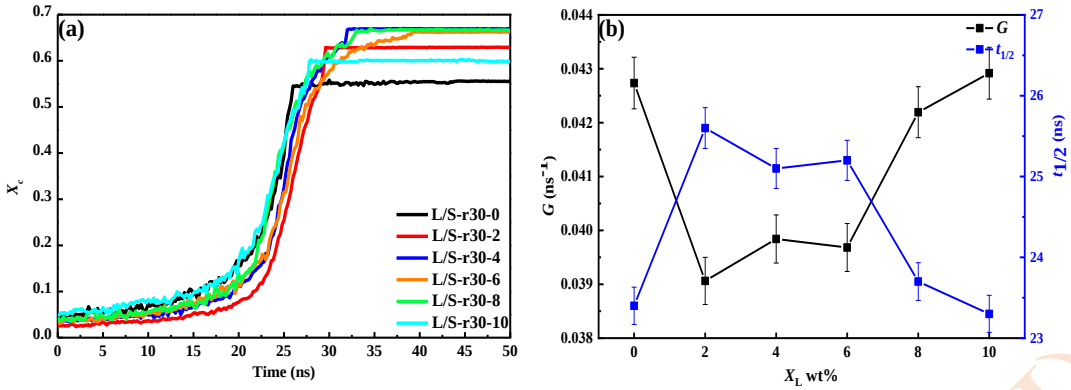

Figure 7. The variation law of (a) crystallinity with time and (b) crystallization rate G and half-crystallization time $t_{1/2}$ with long chain concentration for HDPE/UHMWPE.

Figure 8 shows the curve of tie molecule concentration with time. When the content of long chains is low, the concentration of tie molecules is almost zero in stage I. When the X_L is more than 2 wt%, some unstable tie molecules appear in stage I, which indicates that there is some promotion of nucleation in the long chains. Stable crystal regions begin to appear in the later part of this stage, but the concentration of tie molecules is still very low, which indicates that the nucleation is very dispersed. When the crystal growth stage is reached, the number of crystal regions increases rapidly, and a large number of tie molecules appear in a short time and tend to a certain value.

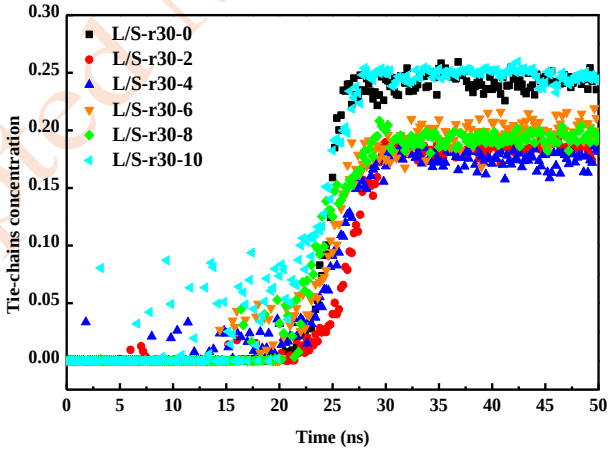

Figure 8. The curves of tie-chains concentration with time for HDPE/UHMWPE with different long chain concentration.

Effect of long chain content on final crystalline morphology

To further investigate the effect of the X_L on the tie molecule density, Figure 9 statistically shows the

variation curves of X_c, P_i, tie-chains density, and the proportion of CH_2 units in the crystalline region of the system at the final moment with the X_L. Overall, with the increase of X_L, both X_c and P_i increase and then decrease, while the tie-chains concentration decreases and then increases. It indicates that when the X_L increases to a certain value, because of the increased number of entanglement points, the crystal region will be relatively dispersed, which is not favorable for the movement of long chains to the growth front to fold and form lamellar crystals. Figure 10 shows the final crystal morphology of HDPE/UHMWPE with different X_L.

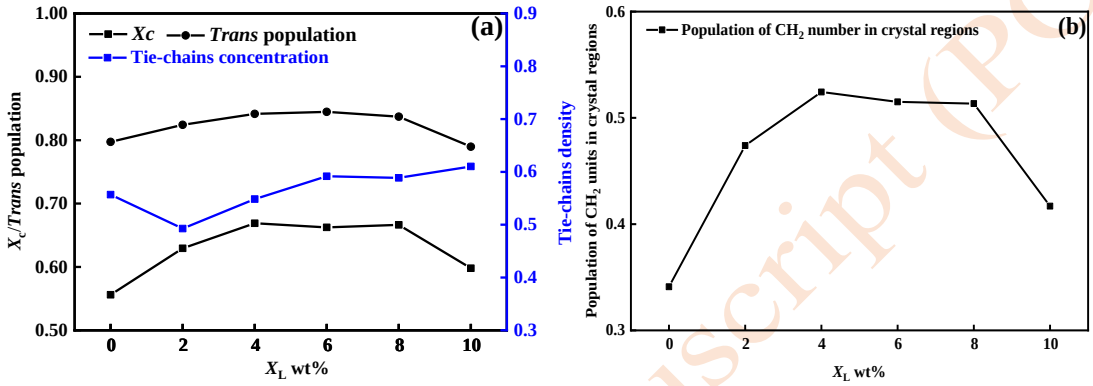

Figure 9. The curves of (a) crystallinity, *trans* state population and tie-chains concentration and (b) population of CH_2 units involved in crystal regions with with long chain concentration.

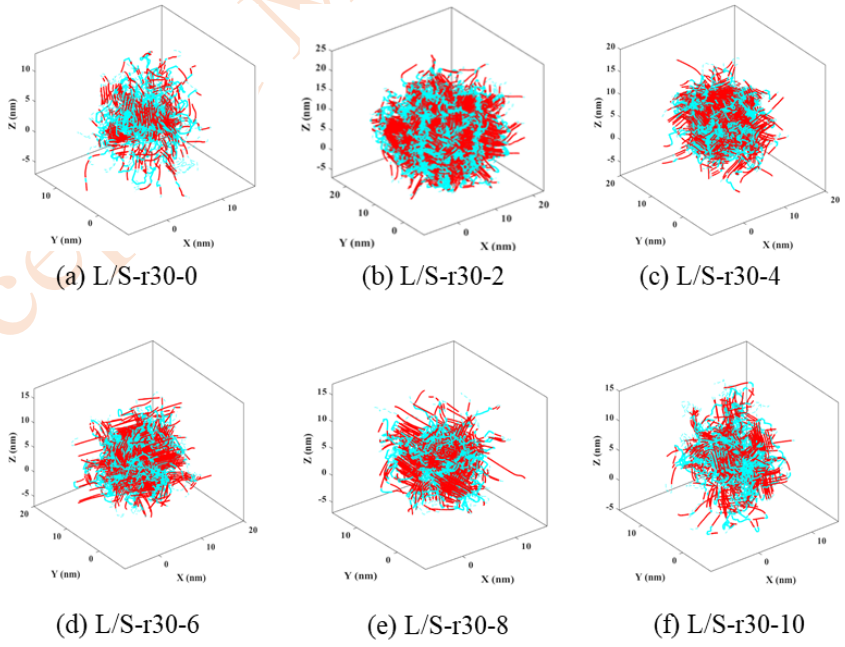

Figure 10. Final crystal structure of HDPE/UHMPWE with different long chain concentration X_L: (a) 0, (b) 2, (c) 4, (d) 6, (e) 8 和 (f) 10 wt%.

Tensile deformation process and mechanism of HDPE/UHMWPE model

Effect of long chain content on tensile deformation at low temperature

In the practical application of HDPE/UHMWPE, strength and rigidity are the most important mechanical properties, so as to judge whether it can meet the requirements of production and life. Here we use the models established above to further simulate the tensile deformation of the system that have experienced static crystallization to study the change mechanism of HDPE/UHMWPE microstructure during the process. The effects of X_L on the mechanical properties and tensile deformation mechanism of the systems at low and high temperature were discussed respectively.

Figure 11 shows the stress-strain curves obtained by uniaxial stretching at lower temperatures for HDPE/UHMWPE systems with different X_L. Taking T = 100 K as an example, the tensile deformation process of all HDPE/UHMWPE models is divided into three stages: (1) elastic deformation stage, the yield strain is basically all around 15%, and the yield stress basically stays around 0.32; (2) plastic deformation stage, the strain is around 15% - 60%; and (3) stress-hardening stage, the stress continues to increase with the strain up to the fracture.

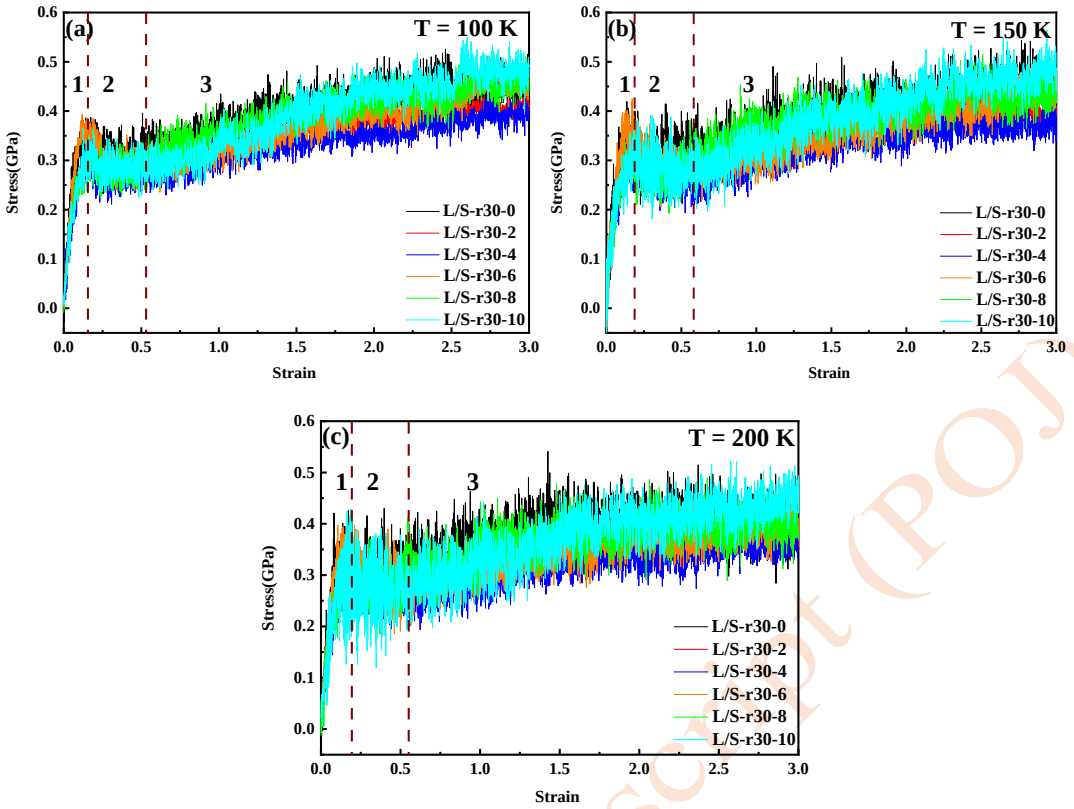

Figure 11. The stress-strain curves for HDPE/UHMWPE with different long chain concentration at different temperature: (a) T = 100 K, (b) T = 150 K and (c) T = 200 K.

Table 3 lists the yield strength, yield strain, elongation at break, tensile strength and toughness of HDPE/UHMWPE with different X_L at T = 100 K. Overall, with the increase of X_L, the yield strength and yield strain decreased slightly, but the tensile strength increased significantly. In addition, elongation at break and material toughness increased and then decreased with increasing X_L, with an optimum value (2 - 4 wt%). The presence of an optimal long chain content can greatly enhance the macroscopic mechanical properties of HDPE matrix polyethylene.

Table 3. Tensile mechanical parameter for HDPE/UHMWPE with different long chain concentration at T= 100 K.

Models	Yield strength (MPa)	Yield strain (%)	Elongation at break (%)	Tensile strength (MPa)	[(a)] Toughness (MPa)
L/S-r30-0	346.9	16.2	323	483.3	1270
L/S-r30-2	319.5	15.5	591	460.2	2280
L/S-r30-4	316.4	15.1	539	495.5	2008
L/S-r30-6	352.6	15.3	352	498.8	1353
L/S-r30-8	310.6	14.6	376	5124.5	1474
L/S-r30-10	305.6	14.8	295	523.4	1112

(a) Toughness is obtained by integrating the stress-strain curve to the fracture point.

Combined with Figure 11 and Table 3, it can be seen that with the increase of long chain content, the yield strength and yield stress are only slightly reduced, which is because the crystallinity of the HDPE/UHMWPE system at low content does not change much, so it still shows the law that the higher the crystallinity is the higher the yield stress is relatively high. At the same time, with the increase of X_L, the tensile strength of the system gradually increases, indicating that the long chains can promote the formation of more oriented crystal regions to resist tensile damage in the process of necking and stress hardening. The elongation at break and toughness also increased significantly after the introduction of long chains. However, after the X_L exceeded 4 wt%, the elongation at break and toughness decreased with the increase of the X_L, which was mainly due to the fact that the excessive introduction of long chains would form more chain entanglements, which was not conducive to the orientation of amorphous tethered molecules in the stress-hardening process.

Effect of long chain content on crystal region parameters during tensile deformation at low temperature

We further investigated the evolution of the crystal region structure during tensile deformation. Figure 12 shows the variation patterns of X_c and P_i with time in the system during tensile deformation at T = 100 K, and the variation pattern of the decrease in crystallinity ($\Delta X_{c|strain=1.0}$) with the X_L when the strain reaches 100%. In stage 1, the X_c and P_i are almost constant. In stage 2 (strain between 15% - 60%), the X_c and P_i keep decreasing as stretching proceeds, which is mainly caused by lamellar dislocation slip followed by stress-induced melt-recrystallization. It can also be in seen that the $\Delta X_{c|strain=1.0}$ is slightly slowed down by the addition of long chains. Stage 3 is the stress-hardening stage, during which there is a plateau in the X_c and P_i, and the X_c rises later in the hardening stage. This is caused by stress-induced

melting of local crystalline regions and reappearance of oriented crystallization. In addition, as the X_L increases, the final X_c first increases and then decreases. This is due to the fact that at low content, the degree of long chain orientation is obvious, which is conducive to orientation nucleation, but with the increase of X_L, the effect of chain entanglement becomes more and more obvious, resulting in a decrease in the X_c. Therefore, the addition of a small amount of long chains can not improve the strength of the material, but can significantly improve the toughness of the material. When the X_L exceeds 4 wt%, the degree of chain entanglement is too great, which causes the formation of oriented lamellae to be hindered, and the elongation at break of the material decreases.

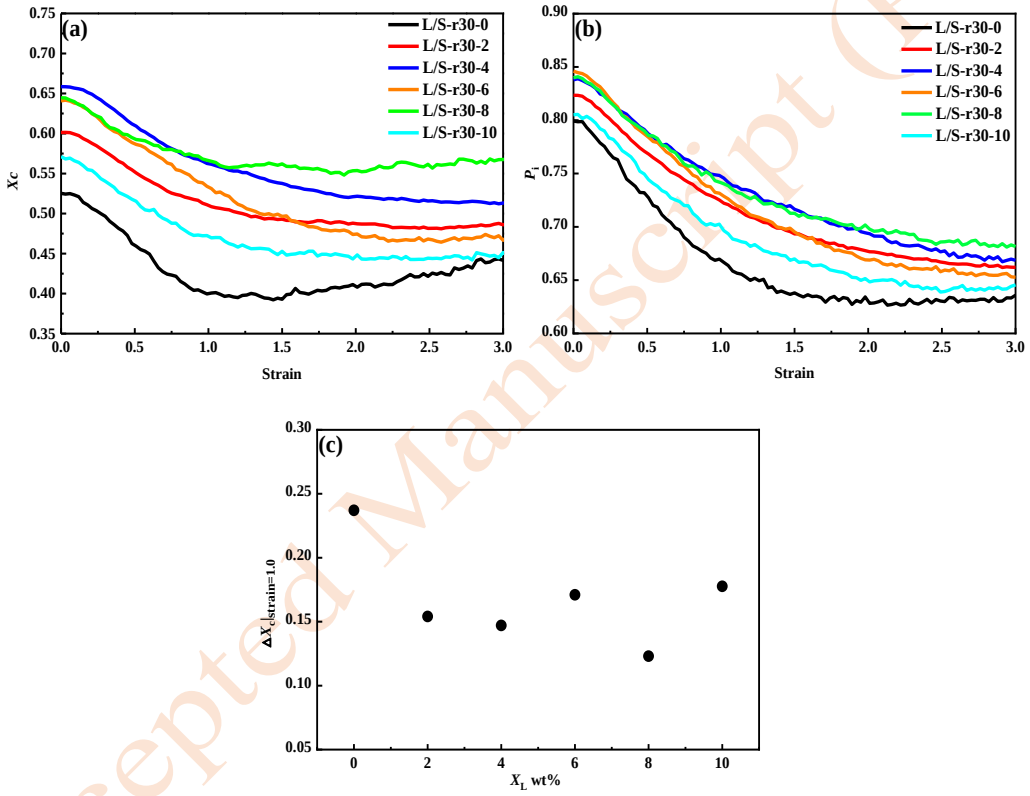

Figure 12. The curves of (a) crystallinity, (b) *trans* state population and (c) normalized number of crystal regions with strain for HDPE/UHMWPE with different long chain concentration as well as crystallinity descent gradient ($\Delta X_{c|strain\ =\ 1.0}$) with long chain concentration when strain reaching at 100% at T = 100 K.

Effect of long chain content on tensile deformation at high temperature

Figure 13 shows the stress-strain curves of HDPE/UHMWPE systems with different long chain concentration at T = 400 K. At high temperatures, the HDPE/UHMWPE system still has obvious elastic deformation of interlamellar bridging molecular chains under tensile action, and the crystals start to

undergo dislocation slip at the yield point (strain near 16%), as well as in the plastic deformation stage (strain from 16% to about 150%), but the stress-hardening behavior is almost invisible. The yield point is relatively more pronounced when the long chain content is 4-6 wt%, as shown in the small diagram in Figure 13.

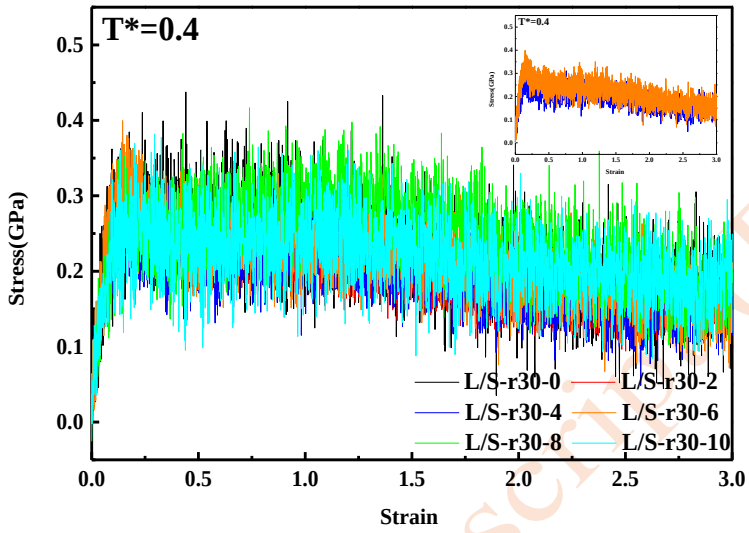

Figure 13. The stress-strain curves for HDPE/UHMWPE with different long chain concentration at T = 400 K.

Figure 14 shows the variation of crystalline region structural parameters such as X_c, P_i, the number of CH_2 units in the crystalline region, and the normalized number of crystal regions with time during stretching at high temperatures. During the yielding stage, a small decrease in the X_c, P_i, and the proportion of CH_2 units in the crystal regions occurs, and dislocation slip damage occurs in the crystal regions. In the subsequent plastic deformation stage, the X_c, P_i, and the proportion of CH_2 units within the crystal region rapidly decrease to the X_c of the system being 0, with only tiny clusters consisting of dispersed *trans*-dihedral angle enriched fragments, and little stress hardening occurs. It can also be seen from Figure 14 that the time taken for the X_c to reach 0 at high temperature stretching becomes gradually longer and the deformation becomes larger with the increase of the X_L, which indicates that the entanglement of long chains plays a hindering role in the stress-induced melting of the lamellar crystals, and that the strain in the crystal region to reach 0 is rather reduced when the X_L is larger than 8 wt%. It is probably due to the fact that excessive long chains are detrimental to the static crystallization process prior to stretching of HDPE/UHMWPE, forming thin lamellar crystals that are more susceptible to stress-induced melting.

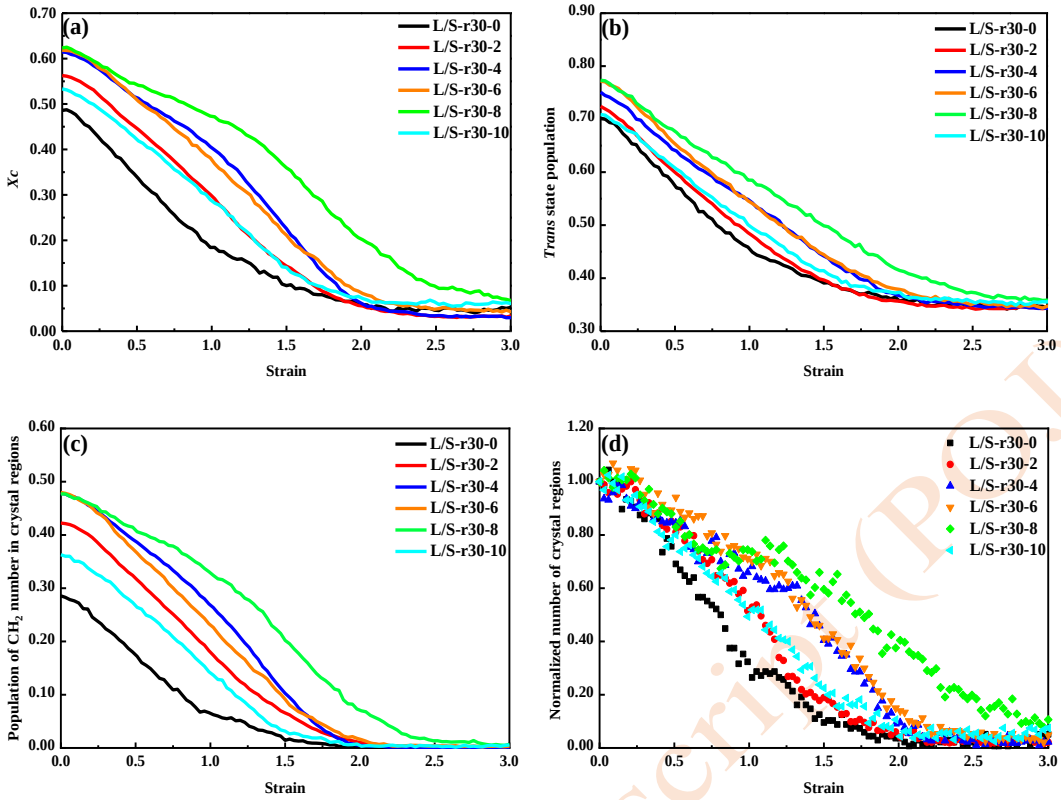

Figure 14. The curves of (a) crystallinity X_c, (b) *trans* state population P_i, (c) population of CH_2 units involved in crystal regions and (d) normalized number of crystal regions with strain for HDPE/UHMWPE with different long chain concentration X_L at T = 400 K.

Effect of temperature on tensile deformation process of HDPE/UHMWPE

The influence of X_L on the tensile deformation process at low and high temperature was analyzed above. For a single model, temperature is also one of the important influencing factors. Figure 15 shows the tensile curves of the models at different temperatures, where the temperature can be divided into low temperature areas (T = 100 K, 150 K and 200 K) and high temperature areas (T = 300 K and 400 K). The responses of different systems to temperature changes are basically the same, so the L/S-r30-4 model is taken as an example to explore the effect of temperature on the tensile failure process.

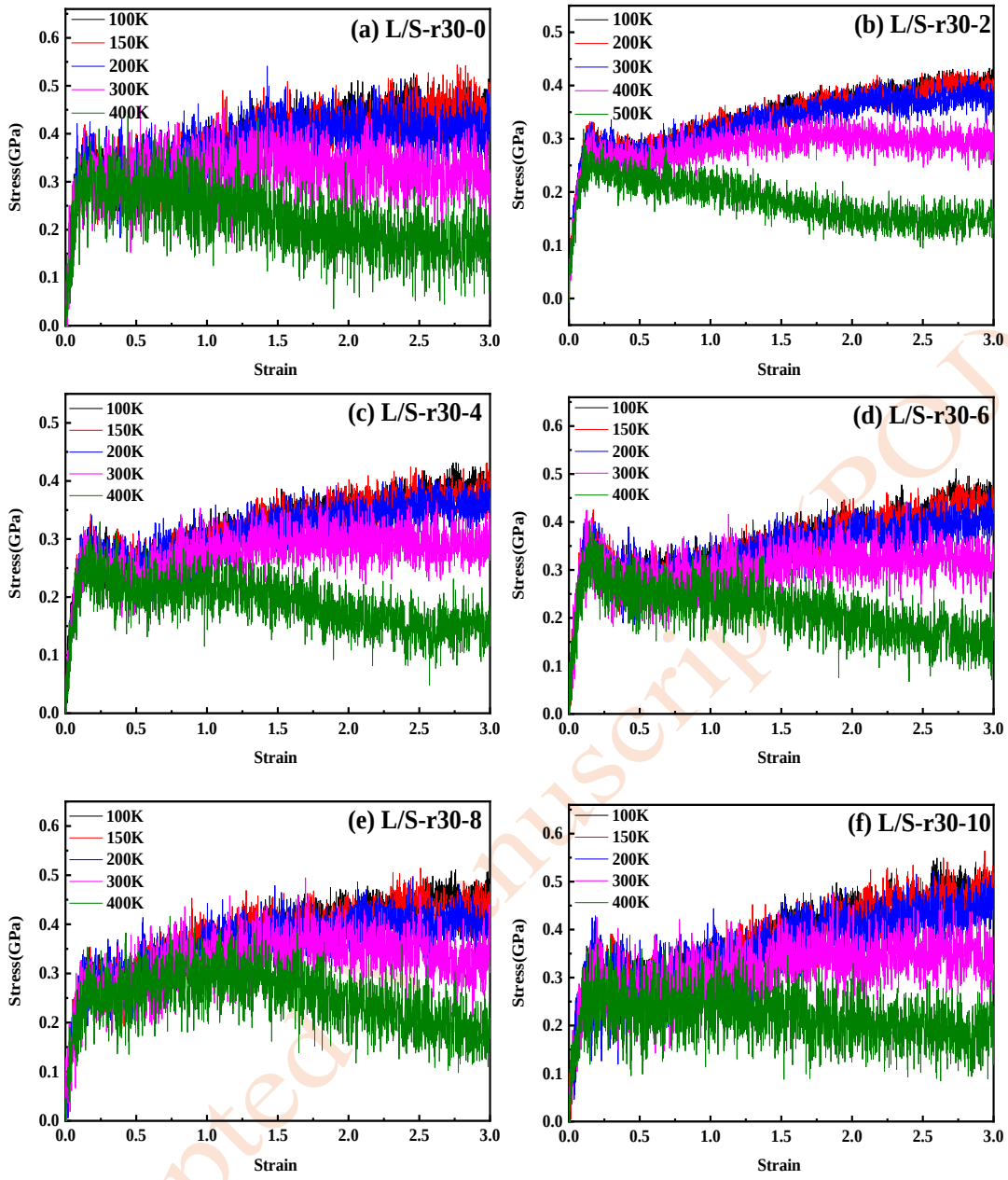

Figure 15. The stress-strain curves for HDPE/UHMWPE models at different temperature: (a) L/S-r30-0, (b) L/S-r30-2, (c) L/S-r30-4, (d) L/S-r30-6, (e) L/S-r30-8 and (f) L/S-r30-10.

Table 4 demonstrates the tensile mechanical parameters of the L/S-r30-4 model at different temperatures. As the temperature raises, the yield point decreases. This is because when the temperature increases, the thermal motion ability of molecular chains is enhanced, and the crystal structure is more prone to damage. Melting occurs inside the crystal, leading to a decrease in the stress value required for material deformation, resulting in lower yield stress. When the tensile temperature belongs to the low-temperature region, as the temperature increases, the elongation at break of the system increases and the tensile strength decreases. When the temperature belongs to the high-temperature region, the melting

phenomenon in the crystal region is obvious, and the elongation at break and tensile strength decrease significantly.

Table 4. Tensile mechanical parameters for L/S-r30-4 at different temperature.

Models	Yield strength (GPa)	Yield strain (%)	Elongation at break (%)	Tensile strength (GPa)	Toughness (GPa)
100K	300.1	15.1	539.3	495.5	2008
150K	285.6	15.0	569.1	481.9	2114
200K	292.1	14.5	575.5	445.6	2000
300K	299.9	14.2	/	/	/
400K	257.7	13.9	/	/	/

Figure 16 shows the variation of tie-chains concentration and number of crystal regions at different temperatures during stretching. From Figure 16, it can be seen that at the fracture, the concentration of tie-chains becomes larger and the number of crystal regions increases slightly with the increase of temperature in the low temperature stretching process. It indicates that at this temperature, a larger number of tie molecules can well disperse the stress, resist the destruction of the crystal regions, and improve the mechanical properties of the system. In addition, in the low-temperature region, when the temperature is slightly higher, it is favorable to accelerate the movement of long chains, which can connect the small crystalline regions to form a perfect amorphous region network. Moreover, at a slightly higher temperature in the hardening stage, the long chains induce the formation of oriented crystallization at a faster rate, accelerating the formation of crystalline regions. In addition, when the temperature is slightly higher, the thermodynamic difference between folded chains and crystalline regions is greatly reduced, which is conducive to the re-arrangement of molecular chains in the amorphous region into the crystal lattice. During the high-temperature stretching process, the concentration of tie molecules and the number of crystal regions decrease significantly. Even when the stretching temperature is 400 K and the deformation reaches 200%, the crystal is completely melted, and the concentration of tie molecules and the number of crystal regions are both 0.

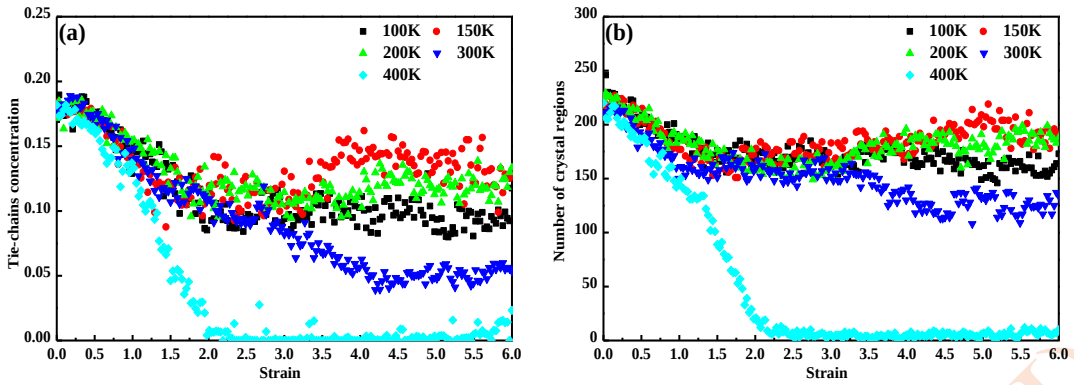

Figure 16. The curves of (a) tie-chains concentration and (b) number of crystal regions with strain for L/S-r30-4 model at different temperature.

Figure 17 statistically plots the variation of X_c, P_i and the proportion of CH_2 units in the crystalline region with strain at different temperatures. In the elastic deformation and yielding stages, the plateau of X_c gradually disappears with the increase of temperature. This indicates that the increase in temperature results in melting in the crystalline region on the one hand and the vulnerability of the crystalline region to damage due to the accelerated molecular motion on the other hand. In the plastic deformation stage, the X_c, P_i, and proportion of CH_2 units in the crystalline region decrease at an accelerated rate with increasing temperature. This indicates that high temperature accelerates molecular chain slip and unraveling. In the subsequent stress-hardening stage, significant melt recrystallization occurs in the low-temperature region, and the X_c remains essentially unchanged near a strain of 200%.

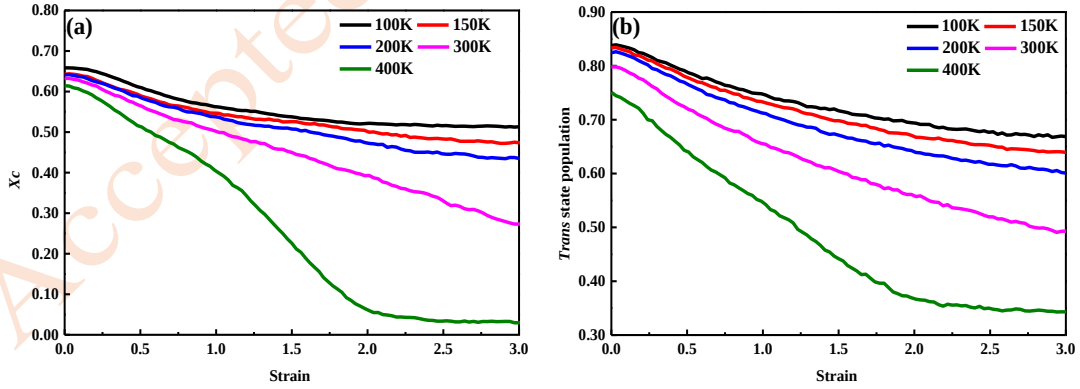

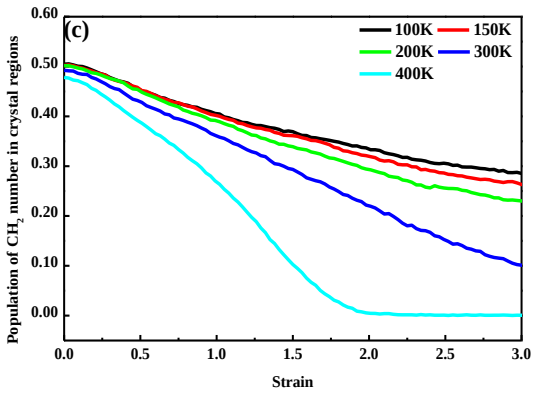

Figure 17. The curves of (a) crystallinity, (b) *trans* state population and (c) population of CH_2 units involved in crystal regions with strain for L/S-r30-4 model at different temperature.

Figure 18 shows the conformation of the L/S-r30-4 model at different temperatures when the tensile strain reaches 300%. It can be clearly seen from the figure that a large number of distinctly oriented crystallizations end up at lower temperatures (100 K, 150 K, and 200 K), while only a few dispersed small crystalline regions are observed at higher temperatures (300 K and 400 K). Moreover, the stress-induced melt-recrystallization forms significantly fewer oriented aligned crystalline regions as the temperature increases.

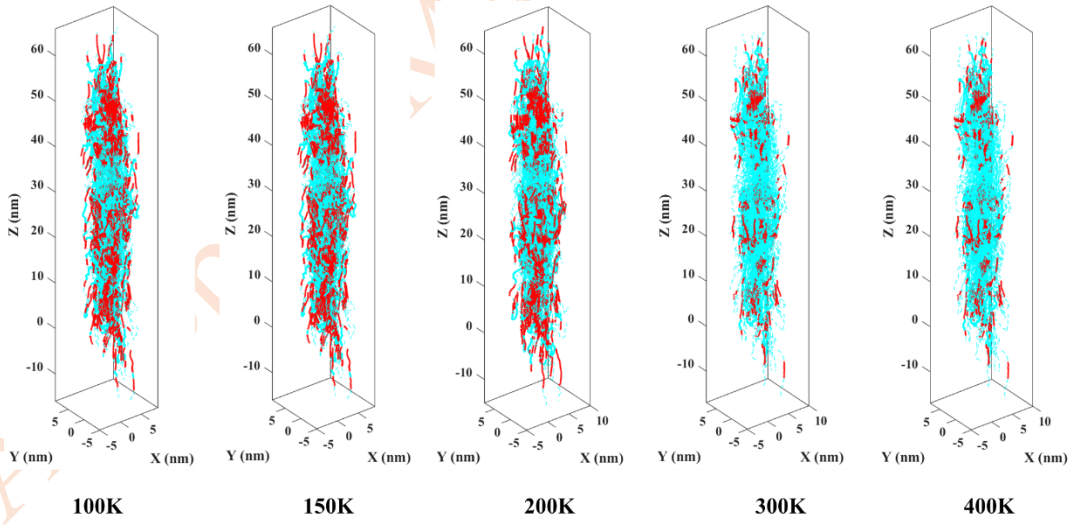

Figure 18. Evolution snapshots of the microstructure of model L/S-r30-2 at different temperature at 300% strain.

CONCLUSIONS

In this work, six models of HDPE/UHMWPE bimodal polyethylene were constructed, and the effect of long chain content on the static crystallization behavior was first explored at the molecular level through

molecular dynamics simulations. At stage I, *trans* dihedral angles were enriched for nucleation. After the chain segments have undergone localized trans enrichment, unstable clusters of small crystalline regions before the nucleation are formed, and these clusters undergo behaviors such as dissipation and merging to gradually form a certain number of stable nuclei. Stage II is the growth stage of small lamellar crystal fragments. During this period the small lamellar crystal fragments continue to grow but do not rapidly form a large number of new crystal regions. Stage III is the stage of rapid fusion of small crystalline fragments, during which fusion of small crystalline regions occurs and a large number of surrounding molecular chain segments fold into the crystalline regions prompting the rapid formation and growth of lamellar crystals. Stage IV is the stabilization stage after the completion of crystallization. The crystal structure reaches perfection, the crystal structure appears to be slightly adjusted, and the crystallization process basically reaches equilibrium. In the static crystallization process, the influence of long chain content is significant. The increase of long chain content can provide more nucleation sites and promote the nucleation rate; in the crystal growth stage, when the long chain content increases to a certain value, the number of entanglement points increases, resulting in the relative dispersion of the crystal region, which is not conducive to the movement of the long chains to the growth front folding to form lamellar crystals.

Subsequently, the effect of long chain content on the tensile deformation behavior was explored. The effect of long chain content on mechanical parameters and microstructure during tensile deformation at low temperature was significant. On the one hand, for the mechanical properties, with the increase of long chain content, the yield strength and yield strain slightly decreased, but the tensile strength significantly increased. At the same time, the elongation at break and material toughness firstly increased and then decreased, and the optimum value (2-4 wt%) existed. On the other hand, for the crystalline region parameters, the final crystallinity increases and then decreases as the long chain content increases. This is due to the fact that at low content, the degree of orientation of long chains is obvious, which is favorable for orientation nucleation. However, as the content of long chains increases, the effect of chain entanglement becomes more and more obvious, resulting in a decrease in crystallinity. At high temperatures, the tensile deformation process is almost free of stress hardening. The addition of long chains on the melting of lamellar crystals have a certain impediment, when the long chain content of 4-6 wt% yield point is relatively obvious. When the content of long chains is greater than 8 wt%, the crystalline structure of the lamellar crystals is thin, and it is easier to occur stress-induced melting and

accelerate the melting of crystals.

The effect of temperature is further explored. In the low-temperature region, there is eventually a large number of distinct oriented crystallites. At the same time, both the melting rate of the crystalline region and the rate of long-chain acceleration-induced formation of crystalline regions increase with increasing temperature, and when the melting rate of the crystalline region is less than the rate of long-chain acceleration-induced formation of crystalline regions, the mechanical properties of the material increase at this temperature, and vice versa, the mechanical properties decrease. In the high-temperature region, the melting of the regions basically dominates, so the crystallinity decreases rapidly and the oriented arrangement of the regions decreases significantly. In summary, this work has focused on a detailed study of the structural changes of the HDPE/UHMWPE system model during crystallization and tensile deformation, and discussed the effects of long chain content and temperature, laying the foundation for actual experiments and production of HDPE/UHMWPE with excellent performance.

ACKNOWEDGEMENTS: This work is financially supported by the National Natural Science Foundation of China (No. 22278141).

REFERENCES

1. Watters EP, Spedding PL, Grimshaw J, Duffy JM, Spedding RL (2005) Wear of artificial hip joint material. Chem Eng J 112: 137-144 [CrossRef]
2. Song S, Wu P, Ye M, Feng J, Yang Y (2008) Effect of small amount of ultra high molecular weight component on the crystallization behaviors of bimodal high density polyethylene. Polymer 49: 2964-2973 [CrossRef]
3. Hofmann D, Kurek A, Thomann R, Schwabe J, Mark S, Enders M, Hees T, Mülhaupt R (2017) Tailored nanostructured HDPE wax/UHMWPE reactor blends as additives for melt-processable all-polyethylene composites and in situ UHMWPE fiber reinforcement. Macromolecules 50: 8129-8139 [CrossRef]
4. Huang YF, Xu JZ, Zhang ZC, Xu L, Li LB, Li JF, Li ZM (2017) Melt processing and structural manipulation of highly linear disentangled ultrahigh molecular weight polyethylene. Chem Eng J 315:132-141 [CrossRef]
5. Farrar DF, Brain AA (1997) The microstructure of ultra-high molecular weight polyethylene used in

total joint replacements. Biomaterials 18: 1677-1685 [CrossRef]

6. Knuuttila H, Lehtinen A, Nummila-Pakarinen A (2004) Advanced polyethylene technologies—controlled material properties. Adv Polym Sci 169: 13-27 [CrossRef]
7. Lim KL, Ishak ZM, Ishiaku US, Fuad AM, Yusof AH, Czigany T, Pukanzsky B, Ogunniyi DS (2006) High density polyethylene/ultra high molecular weight polyethylene blend. II. Effect of hydroxyapatite on processing, thermal, and mechanical properties. J Appl Polym Sci 100: 3931-3942 [CrossRef]
8. Zou H, Chen Y, Liang M (2014) Dynamic rheological behavior of polyethylene/ultra-high-molecular-weight polyethylene blends. Chin Polymer Bulletin 2: 130-136
9. Kurtz SM, Muratoglu OK, Evans M, Edidin AA (1999) Advances in the processing, sterilization, and crosslinking of ultra-high molecular weight polyethylene for total joint arthroplasty. Biomaterials 20: 1659-1688 [CrossRef]
10. Bohm LL, Enderle HF, Fleißner M (1992) High-density polyethylene pipe resins. Adv Mater 4: 234-238 [CrossRef]
11. Moreno J, Paredes B, Carrero A, Vélez D (2017) Production of bimodal polyethylene on chromium oxide/metallocene binary catalyst: Evaluation of comonomer effects. Chem Eng J 315: 46-57 [CrossRef]
12. Gholami F, Pircheraghi G, Rashedi R, Sepahi A (2019) Correlation between isothermal crystallization properties and slow crack growth resistance of polyethylene pipe materials. Polymer Testing 80: 106128 [CrossRef]
13. Xu L, Huang YF, Xu JZ, Ji X, Li ZM (2014) Improved performance balance of polyethylene by simultaneously forming oriented crystals and blending ultrahigh-molecular-weight polyethylene. RSC Advances 4:1512-1520 [CrossRef]
14. Wang YL, Zun Q (2018) A Study on the Flowability and Mechanical Properties of UHMWPE/HDPE Blends. China Plastics Industry 5: 18-20
15. Hoffman JD, Miller RL. Kinetic of crystallization from the melt and chain folding in polyethylene fractions revisited: theory and experiment. Polymer 38: 3151-3212 [CrossRef]
16. Strobl G (2006) Crystallization and melting of bulk polymers: New observations, conclusions and a thermodynamic scheme. Prog polym Sci 31: 398-442 [CrossRef]
17. Strobl G (2009) Colloquium: Laws controlling crystallization and melting in bulk polymers. Rev

Mod Phys 81: 1287-1300 [CrossRef]

18. Chen Y, Zou H, Liang M, Liu P (2013) Study on the dynamic rheological behavior of four different bimodal polyethylenes. J Macromolecular Sci-B 52: 924-936 [CrossRef]
19. Yang L, Somani RH, Sics I, Hsiao BS, Kolb R, Fruitwala H, Ong C (2004) Shear-induced crystallization precursor studies in model polyethylene blends by in-situ rheo-SAXS and rheo-WAXD. Macromolecules 37: 4845-4859 [CrossRef]
20. Hsiao B, Yang L, Somani R, Zhu L (2005) Unexpected Shish-Kebab Structure in Shear-Induced Polyethylene Melt. In: APS March Meeting Abstracts, pp. X30-007
21. Zhao L, Hu Y, Shao Y, Liu Z, Liu B, He X. Molecular dynamics simulation of shish-kebab crystallization of polyethylene: Unraveling the effects of molecular weight distribution. The J Chem Phys150: 184114-184114 [CrossRef]
22. Lv F, Chen X, Wan C, Su F, Ji Y, Lin Y, Li X, Li L (2017) Deformation of ultrahigh molecular weight polyethylene precursor fiber: crystal slip with or without melting. Macromolecules 50: 6385-6395 [CrossRef]
23. Yang F, Gao H, Hu W (2012) Monte Carlo simulations of crystallization in heterogeneous copolymers: The role of copolymer fractions with intermediate comonomer content. J Mater Res 27: 1383-1388 [CrossRef]
24. Nie Y, Zhao Y, Matsuba G, Hu W (2018) Shish-kebab crystallites initiated by shear fracture in bulk polymers. Macromolecules 51: 480-487 [CrossRef]
25. Guan X, Wang Y, Wang J, Wu Y, Hu W (2019) Effects of short-chain branches on strain-induced polymer crystallization. Polym Int 68: 225-230 [CrossRef]
26. Hu Y, Shao Y, Liu Z, He X, Liu B (2019) Dominant effects of short-chain branching on the initial stage of nucleation and formation of tie chains for bimodal polyethylene as revealed by molecular dynamics simulation. Polymers 11: 1840 [CrossRef]
27. Jeong S, Kim JM, Cho S, Baig C (2017) Effect of short-chain branching on interfacial polymer structure and dynamics under shear flow. Soft Matter 14: 470 [CrossRef]
28. Sanmartín S, Ramos J, Vega JF, Martínez-Salazar J (2014) Strong influence of branching on the early stage of nucleation and crystal formation of fast cooled ultralong n-alkanes as revealed by computer simulation. Eur Polym J 50: 190-199 [CrossRef]
29. Lee S, Rutledge GC (2011) Plastic deformation of semicrystalline polyethylene by molecular

simulation. Macromolecules 44: 3096-3108 [CrossRef]

30. Kim JM, Locker R, Rutledge G (2014) Plastic deformation of semicrystalline polyethylene under extension, compression, and shear using molecular dynamics simulation. Macromolecules 47: 2515-2528 [CrossRef]
31. Yeh IC, Andzelm JW, Rutledge GC (2015) Mechanical and structural characterization of semicrystalline polyethylene under tensile deformation by molecular dynamics simulations. Macromolecules 48: 4228-4239 [CrossRef]
32. Yeh IC, Lenhart JL, Rutledge GC, Andzelm JW (2017) Molecular dynamics simulation of the effects of layer thickness and chain tilt on tensile deformation mechanisms of semicrystalline polyethylene. Macromolecules 50: 1700-1712 [CrossRef]
33. Ranganathan R, Kumar V, Brayton AL, Kroger M, Rutledge GC. Atomistic modeling of plastic deformation in semicrystalline polyethylene: Role of interphase topology, entanglements, and chain dynamics. Macromolecules 53: 4605-4617 [CrossRef]
34. Hossain D, Tschopp MA, Ward DK, Bouvard JL, Wang P, Horstemeyer MF (2010) Molecular dynamics simulations of deformation mechanisms of amorphous polyethylene. Polymer 51: 6071-6083 [CrossRef]
35. Zhao L, Hu Y, Shao Y, Liu Z, Liu B, He X (2019) Molecular dynamics simulation of shish-kebab crystallization of polyethylene: Unraveling the effects of molecular weight distribution. J Chem Phys 150: 184114 [CrossRef]
36. Hu Y, Shao Y, Liu Z, He X, Liu B (2019) Dominant effects of short-chain branching on the initial stage of nucleation and formation of tie chains for bimodal polyethylene as revealed by molecular dynamics simulation. Polymers 11: 1840 [CrossRef]
37. Chatterjee AK, Morgan JP, Scholl M, Grubbs RH (2000) Synthesis of functionalized olefins by cross and ring-closing metatheses. J Am Chem Soc 122: 3783-3784 [CrossRef]
38. Natta G (1959) Kinetic studies of α-olefin polymerization. J Polym Sci 34: 21-48 [CrossRef]
39. Kaminsky W (2004) The discovery of metallocene catalysts and their present state of the art. J Polym Sci Pol Chem 42: 3911-3921 [CrossRef]
40. Agapie T (2011) Selective ethylene oligomerization: Recent advances in chromium catalysis and mechanistic investigations. Coord Chem Rev 255:861-880 [CrossRef]
41. Mayo SL, Olafson BD, Goddard WA (1990) DREIDING: a generic force field for molecular

simulations. J Phys Chem 94: 8897-8909 [CrossRef]

42. Yu X, Kong B, Yang X (2008) Molecular dynamics study on the crystallization of a cluster of polymer chains depending on the initial entanglement structure. Macromolecules 63: 197-204 [CrossRef]
43. Jordens K, Wilkes GL, Janzen J, Rohlfing DC, Welch MB (2000) The influence of molecular weight and thermal history on the thermal, rheological, and mechanical properties of metallocene-catalyzed linear polyethylenes. Polymer 41: 7175-7192 [CrossRef]
44. Lavine MS, Waheed N, Rutledge GC (2003) Molecular dynamics simulation of orientation and crystallization of polyethylene during uniaxial extension. Polymer 44: 1771-1779 [CrossRef]
45. Balzano L, Rastogi S, Peters GW (2009) Crystallization and precursors during fast short-term shear. Macromolecules 42: 2088-2092 [CrossRef]
46. Fernandez-Ballester L, Thurman DW, Zhou W, Kornfield JA (2012) Effect of long chains on the threshold stresses for flow-induced crystallization in iPP: Shish kebabs vs sausages. Macromolecules 45: 6557-6570 [CrossRef]
47. Jabbari-Farouji S, Rottler J, Lame O, Makke A, Perez M, Barrat JL (2015) Plastic deformation mechanisms of semicrystalline and amorphous polymers. ACS Macro Lett [CrossRef]
48. Gao R, He X, Shao Y, Hu Y, Zhang H, Liu Z, Liu B (2016) Effects of branch content and branch length on polyethylene crystallization: Molecular dynamics simulation. Macromol Theory Simul 25: 303-311 [CrossRef]
49. Yamamoto T (2019) Molecular dynamics simulation of stretch-induced crystallization in polyethylene: Emergence of fiber structure and molecular network. Macromolecules 52: 1695-706 [CrossRef]
50. Cao Y, Zhao L, Wang J, Shao Y, He X (2021) Molecular dynamics simulation of extension-induced crystallization of branched bimodal HDPE: Unraveling the effects of short-chain branches. Phys Chem Chem Phys 23: 19862–19871 [CrossRef]
51. Gilbert M, Hybart FJ (1972) Effect of chemical structure on crystallization rates and melting of polymers: Part 1. Aromatic polyesters. Polymer 13: 327-332 [CrossRef]